Dynamo onset as a first-order transition: Lessons from a shell model for magnetohydrodynamics

Ganapati Sahoo,[1,*] Dhrubaditya Mitra,[2,†] and Rahul Pandit[1,‡]

[1]*Department of Physics, Centre for Condensed Matter Theory, Indian Institute of Science, Bangalore 560012, India*

[2]*Astronomy Unit, School of Mathematical Sciences, Queen Mary College, University of London, London E1 4NS, United Kingdom*

We carry out systematic and high-resolution studies of dynamo action in a shell model for magnetohydrodynamic (MHD) turbulence over wide ranges of the magnetic Prandtl number Pr_M and the magnetic Reynolds number Re_M. Our study suggests that it is natural to think of dynamo onset as a nonequilibrium first-order phase transition between two different turbulent, but statistically steady, states. The ratio of the magnetic and kinetic energies is a convenient order parameter for this transition. By using this order parameter, we obtain the stability diagram (or nonequilibrium phase diagram) for dynamo formation in our MHD shell model in the (Pr_M^{-1}, Re_M) plane. The dynamo boundary, which separates dynamo and no-dynamo regions, appears to have a fractal character. We obtain a hysteretic behavior of the order parameter across this boundary and suggestions of nucleation-type phenomena.

PACS number(s): 47.27.Gs, 47.65.−d, 05.45.−a

I. INTRODUCTION

The elucidation of dynamo action is a problem of central importance in nonlinear dynamics because it has implications for a variety of physical systems. Dynamo instabilities, which amplify weak magnetic fields in a turbulent conducting fluid, are believed to be the principal mechanism for the generation of magnetic fields in celestial bodies and in the interstellar medium [1–7], and in liquid-metal systems [8–13] studied in laboratories. In these situations the kinematic viscosity ν and the magnetic diffusivity η can differ by several orders of magnitude, so the magnetic Prandtl number $Pr_M \equiv \nu/\eta$ can either be very small or very large, e.g., $Pr_M \simeq 10^{-2}$ at the base of the Sun's convection zone, $Pr_M \simeq 10^{-5}$ in the liquid-sodium system, and $Pr_M \simeq 10^{14}$ in the interstellar medium. This Prandtl number is related to the Reynolds number $Re = UL/\nu$ and the magnetic Reynolds number $Re_M = UL/\eta$ that characterize the conducting fluid; here L and U are typical length and velocity scales in the flow; clearly $Pr_M = Re_M/Re$.

Two dissipative scales play an important role here; they are the Kolmogorov scale ℓ_d ($\sim \nu^{3/4}$ at the level of Kolmogorov 1941 (K41) phenomenology [14]) and the magnetic-resistive scale ℓ_d^M ($\sim \eta^{3/4}$ in K41). For large Prandtl numbers, i.e., $Pr_M \gg 1$, $\ell_d^M \ll \ell_d$ so the magnetic field grows predominantly in the dissipation range of the fluid until it is strong enough to affect the dynamics of the fluid through the Lorentz force. This behavior is a characteristic of a small-scale turbulent dynamo, in which dynamo action is driven by a smooth dissipative-scale velocity field. In the initial stage of growth, called the kinematic stage of the dynamo, the magnetic field is not large enough to act back on the velocity field. Dynamo action can be obtained for values of Re_M that are large enough to overcome Joule dissipation; and the

dynamo-threshold value Re_{Mb} decreases as Pr_M increases [15,16]. $Pr_M \simeq 10^{-5}$ in liquid-metal flows [10,13,17] so they lie in the small-Prandtl-number region, $Pr_M \ll 1$, for which the growth of the magnetic energy occurs initially in the *inertial scales* of fluid turbulence, because $\ell_d \ll \ell_d^M$; here the velocity field is not smooth and the local strain rate is not uniform: at the K41 level the turnover velocity of an eddy of size ℓ is $v(\ell) \sim \ell^{1/3}$, so the rate of shearing $[v(\ell)/\ell] \sim \ell^{-2/3}$.

Direct numerical simulations (DNS) are playing an increasingly important role in developing an understanding of such dynamo action. Most DNS studies of MHD turbulence [16,18–20] have been restricted, because of computational constraints, either to low resolutions or to the case $Pr_M = 1$; small-scale dynamos with $Pr_M \gg 1$ have also been studied via DNS [7]. However, given the large range spanned by Pr_M in the physical settings mentioned above, some recent DNS studies of the MHD equations have started to explore the Pr_M dependence of dynamo action; the range of Pr_M covered by such pure DNS studies [16,21] is quite modest ($10^{-2} \lesssim Pr_M \lesssim 10$). To explore the dynamo boundary in the (Pr_M^{-1}, Re_M) plane over a large range of Pr_M, one recent study [16] has used a combination of numerical methods, some of which require small-scale models such as large-eddy simulations (LES) or Lagrangian-averaged MHD (LAMHD), and others, such as a pseudospectral DNS, in which the only approximations are the finite number of collocation points and the finite step used in time marching; yet another DNS study [22] has introduced hyperviscosity of order 8 to study the low Pr_M regime; by using this combination of methods these studies have been able to cover the range $10^{-2} \lesssim Pr_M \lesssim 10^3$ and to obtain the boundary between dynamo and no-dynamo regions but with fairly large error bars.

We have carried out extensive high-resolution numerical studies that have been designed to explore in detail the boundary between the dynamo and no-dynamo regimes in the (Pr_M^{-1}, Re_M) plane in a shell model for three-dimensional MHD [23–26]. This shell model allows us to explore a much larger range of Pr_M than is possible if we use the MHD equations. Although our study uses a simple shell model, it has the virtue that it can explore the boundary between dy-

namo and no-dynamo regions in great detail without resorting to the modeling of small spatial scales. Shell-model studies of dynamo action have also been attempted in Refs. [24,27–29] but these have concentrated on aspects of the dynamo problem that are different from those we consider here.

Our study suggests that it is natural to think of the boundary between dynamo and no-dynamo regimes in the (Pr_M^{-1}, Re_M) plane as a first-order phase boundary that is the locus of first-order nonequilibrium phase transitions from one nonequilibrium statistical steady state (NESS) to another. The first NESS is a turbulent, but statistically steady, conducting fluid in which the magnetic energy is negligibly small compared to the kinetic energy; the second NESS is also a statistically steady turbulent state but one in which the magnetic energy is comparable to the kinetic energy. Indeed, the ratio of the magnetic and fluid energies E_b/E_u turns out to be a convenient order parameter for this nonequilibrium phase transition since it vanishes in the no-dynamo phase and assumes a finite nonzero value in the dynamo state. The other intriguing result of our study is that the boundary between these phases is very intricate and might well have a fractal character; this provides an appealing explanation for the large error bars in earlier attempts to determine this boundary [16,27]. The analogy with first-order transitions that we have outlined above is not superficial. As in any first-order transition we find that our order parameter shows hysteretic behavior [30] as we scan through the dynamo boundary by changing the forcing term at a nonzero rate. We also find some evidence of nucleation-type phenomena: the closer we are to the dynamo boundary, the longer it takes for a significant magnetic field to nucleate and thus lead to dynamo action. We compare our results with earlier studies such as Ref. [31], which have suggested that dynamo action occurs because of a subcritical bifurcation.

The remaining part of this paper is organized as follows: in Sec. II we describe the shell model for MHD [23–25] and the numerical method we employ. Section III is devoted to our results and Sec. IV contains a concluding discussion.

II. MODELS AND NUMERICAL METHODS

To study dynamo action it is natural to use the equations of magnetohydrodynamics (MHD). In three dimensions the MHD equations are

$$\frac{\partial \vec{u}}{\partial t} + (\vec{u} \cdot \nabla)\vec{u} = \nu \nabla^2 \vec{u} - \nabla \bar{p} + \frac{1}{4\pi}(\vec{b} \cdot \nabla)\vec{b} + \vec{f}, \quad (1)$$

$$\frac{\partial \vec{b}}{\partial t} = \nabla \times (\vec{u} \times \vec{b}) + \eta \nabla^2 \vec{b}, \quad (2)$$

where ν and η are the kinematic viscosity and the magnetic diffusivity, respectively, the effective pressure $\bar{p} = p + (b^2/8\pi)$, and p is the pressure. For low-Mach-number flows, to which we restrict ourselves, we use the incompressibility condition $\nabla \cdot \vec{u}(\vec{x}, t) = 0$; and $\nabla \cdot \vec{b}(\vec{x}, t) = 0$.

As we have mentioned above, a DNS of the MHD equations poses a significant computational challenge, even on

the most powerful computers available today, if we want to cover a large part of the (Pr_M^{-1}, Re_M) plane and to locate the dynamo boundary accurately. Therefore, one study [16] has used a combination of LES, LAMHD, and DNS to obtain this boundary. We employ a complementary strategy: we use a simple shell model for MHD [23–25] that allows us to carry out very extensive numerical simulations to probe the nature of the dynamo boundary without using LES or LAMHD.

Shell models comprise a set of ordinary differential equations with nonlinear coupling terms that mimic the advection terms in and respect the shell-model analogs of the conservation laws of the parent hydrodynamic equations in the inviscid, unforced limit [32,33]. For the case of MHD each shell n is characterized by a complex velocity u_n and a complex magnetic field b_n in a logarithmically discretized Fourier space with wave vectors k_n; furthermore, there is a direct coupling only between velocities and magnetic fields in nearest and next-nearest-neighbor shells. The MHD shell model equations [23,24] are

$$\frac{du_n}{dt} = -\nu k_n^2 u_n + i[A_n(u_{n+1}u_{n+2} - b_{n+1}b_{n+2}) + B_n(u_{n-1}u_{n+1}$$
$$- b_{n-1}b_{n+1}) + C_n(u_{n-2}u_{n-1} - b_{n-2}b_{n-1})]^* + f_n^u, \quad (3)$$

$$\frac{db_n}{dt} = -\eta k_n^2 b_n + i[D_n(u_{n+1}b_{n+2} - b_{n+1}u_{n+2}) + E_n(u_{n-1}b_{n+1}$$
$$- b_{n-1}u_{n+1}) + F_n(u_{n-2}b_{n-1} - b_{n-2}u_{n-1})]^* + f_n^b, \quad (4)$$

where $*$ denotes complex conjugation, $1 \leq n \leq N$, with N the total number of shells, the wave numbers $k_n = k_0 2^n$, with $k_0 = 2^{-4}$, and f_n^u and f_n^b the forcing terms in the equations for u_n and b_n, respectively. In our studies of dynamo action, we set $f_n^b = 0$. The parameters $A_n, B_n, \ldots, F_n$, are obtained by demanding that these equations conserve all the shell-model analogs of the invariants of 3DMHD, in the inviscid unforced case, and reduce to the well-known Gledzer-Ohkitani-Yamada (GOY) shell model [32,33] for fluid turbulence if $b_n = 0, \forall n$. In particular, to ensure the conservation of shell-model analogs of the total energy $E_T = E_u + E_b \equiv (1/2)\Sigma_n(|u_n|^2 + |b_n|^2)$, cross helicity $H_C \equiv (1/2)\Sigma_n(u_n b_n^* + u_n^* b_n)$, and magnetic helicity $H_M \equiv \Sigma_n(-1)^n |b_n|^2/k_n$, in the unforced and inviscid case, and to obtain the GOY-model limit for the fluid, we choose

$$A_n = k_n, \quad B_n = -k_{n-1}/2, \quad C_n = -k_{n-2}/2,$$
$$D_n = k_n/6, \quad E_n = k_{n-1}/3, \quad F_n = -2k_{n-2}/3. \quad (5)$$

The only adjustable parameters are the forcing terms and ν and η. The ratio ν/η yields the magnetic Prandtl number Pr_M. The Grashof numbers yield nondimensionalized forces [34] but, for easy comparison with earlier studies [7,16,20,21,27,29], we use the fluid and magnetic Reynolds numbers whose shell-model analogs are, respectively, $Re = u_{rms}\ell_I/\nu$, where $\ell_I = \Sigma(u_n^2/k_n^2)/\Sigma(u_n^2/k_n)$ is the shell-model integral scale, $u_{rms} = \sqrt{\Sigma(u_n^2/k_n)}/\ell_0$, $\ell_0 = 2\pi/k_1$, and $Re_M = Pr_M Re$.

We use the following boundary conditions:

$$A_{N-1} = A_N = B_1 = B_N = C_1 = C_2 = 0,$$

$$D_{N-1} = D_N = E_1 = E_N = F_1 = F_2 = 0. \quad (6)$$

We set $N=30$ and use a fifth-order Adams-Bashforth scheme for solving the shell-model equations; i.e., for an equation of the type

$$\frac{dq}{dt} = -\alpha q + f(t), \quad (7)$$

we use

$$q(t+\delta t) = e^{-2\alpha\delta t} q(t-\delta t) + \frac{1-e^{-2\alpha\delta t}}{24\alpha} [55f(t) - 59f(t-\delta t)$$

$$+ 37f(t-2\delta t) - 9f(t-3\delta t)], \quad (8)$$

where δt is the time step. We have found that this numerical scheme works well for the integration of Eqs. (3) and (4) so long as $N \lesssim 35$ and $\mathrm{Re} \lesssim 10^9$. In all our calculations we use $\delta t = 10^{-4}$. Characteristic time scales include the time scale for diffusion $\tau_\eta = \ell_0^2/\eta$ and the large-eddy-turnover time $\tau_L = \ell_0/u_{\mathrm{rms}}$, where $\ell_0 \equiv 2\pi/k_1$ is the box-size length scale and u_{rms} is the root-mean-square velocity.

The initial conditions we use are as follows: we first obtain a statistically steady state for the GOY-shell-model equations, which are obtained from Eq. (3) by setting all $b_n = 0$; the forcing terms are chosen to be $f_n^u = f_0(1+i)\delta_{n,1}$, with $f_0 = 5.0 \times 10^{-3}$ in all our runs, except ones in which we study hysteretic behavior, and $f_n^b = 0$. We choose the GOY-model shell velocities at time $t=0$ to be $u_n = k_n^{-1/3} \exp(i\varphi_n)$, with φ_n a random phase distributed uniformly on the interval $[0, 2\pi)$. To make sure we have a statistically steady state we evolve the shell velocities u_n until $t = 5 \times 10^5$. This yields the shell-model energy spectrum $E_u(k_n) \equiv |u_n|^2/k_n$ that has the K41 form $\sim k_n^{-5/3}$ if we ignore intermittency corrections. We now introduce a small seed magnetic field, which is such that $E_b \simeq 10^{-28}$, and then follow the temporal evolution of u_n and b_n that is given by Eqs. (3) and (4).

III. RESULTS

Given the numerical scheme that we have described in the previous section, we obtain the time series for u_n and b_n from the MHD-shell-model equations. An analysis of these time series shows two types of NESSs. We refer to the first as the no-dynamo state and to the second as the dynamo state. These states have been found in several earlier studies such as Refs. [7,16,18–21,27]. Our main goal is to explore in detail the phase boundary between these two states. This can be done most easily by the introduction of a dynamo order parameter a natural candidate for which is the ratio E_b/E_u, where the fluid and magnetic energies are, respectively, $E_u = \frac{1}{2}\Sigma_n |u_n|^2$ and $E_b = \frac{1}{2}\Sigma_n |b_n|^2$. Representative plots of this order parameter are given as functions of time t in Fig. 1: the blue dashed curve shows the evolution of E_b/E_u in the dynamo regime; note that here the dynamo order parameter rises rapidly, fluctuates significantly for $t/\tau_\eta \lesssim 2 \times 10^{-4}$, and finally reaches a statistical steady state with equipartition, i.e., $E_b/E_u \simeq 1$. The red full curve in the inset of Fig. 1 shows
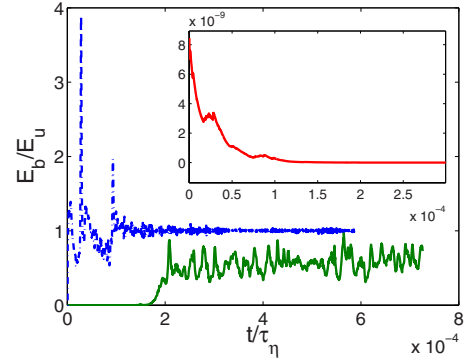

FIG. 1. (Color online) Representative plots of the dynamo order parameter E_b/E_u versus time t/τ_η, with τ_η the magnetic-diffusion time, in the dynamo region (blue dashed curve), near the dynamo boundary (green full line), and in the no-dynamo regime (red full line in the inset).

how E_b/E_u vanishes rapidly in the no-dynamo state. The behavior of the dynamo order parameter is more complicated than these two simple possibilities in the vicinity of the phase boundary between dynamo and no-dynamo states as shown by the green full curve in Fig. 1; E_b/E_u rises much more slowly from zero than in the dynamo regime and then it fluctuates significantly for a long time; the difficulty of pinpointing the dynamo boundary is a consequence of these fluctuations.

The time series for the dynamo order parameter are obtained from those for E_u and E_b; representative plots for these are shown, via red full lines and blue dashed curves, respectively, in Figs. 2(a)–2(f) for a very large range of magnetic Prandtl numbers, namely, $\mathrm{Pr}_M = 10^2, 1, 10^{-1}, 10^{-2}, 10^{-3}$, and 10^{-4}, respectively. The values of ν are (a) 10^{-3}, (b) 10^{-5}, (c) 10^{-6}, (d) 10^{-5}, (e) 10^{-5}, and (f) 10^{-6}; and the corresponding values of the diffusion time scale $\tau_\eta = \ell_0^2/\eta \simeq 2.52 \times 10^8$, 2.52×10^8, 2.52×10^8, 2.52×10^6, 2.52×10^5, and 2.52×10^5, respectively. Clearly dynamo action occurs in Figs. 2(a)–2(d) but not in Figs. 2(e) and 2(f). By obtaining many such plots we can identify the dynamo boundary in the $(\mathrm{Pr}_M^{-1}, \mathrm{Re}_M)$ plane as we will discuss later.

In the dynamo regime the shell-model kinetic and magnetic energy spectra defined, respectively, by $E_u(k_n) \equiv |u_n|^2/k_n$ and $E_b(k_n) \equiv |b_n|^2/k_n$ evolve as shown in Fig. 3. In particular, in Figs. 3(a)–3(c) for $\mathrm{Pr}_M = 10^{-2}, 1$, and 10^2, respectively, we show the evolution of $E_b(k_n)$ with time: the curves with red stars, green diamonds, blue hexagons, cyan circles, and magenta triangles are obtained, respectively, for $t = 1, 5, 10, 15$, and 100; the analogs of these plots for $E_u(k_n)$ are given in Figs. 3(d)–3(f). Note that the initial growth of $E_b(k_n)$ occurs principally at large values of k_n if Pr_M is large; i.e., we have a small-scale dynamo; this growth of $E_b(k_n)$ moves to low values of k_n as Pr_M decreases; earlier studies [19,27] have observed similar trends but not over the large range of Pr_M we cover. As $E_b(k_n)$ grows, the velocity spectra also change but much less than their magnetic counterparts as can be seen by comparing Figs. 3(d)–3(f) with Figs. 3(a)–3(c), respectively. In all these plots the curves with black squares indicate $E_u(k_n)$ from the initial steady state for the GOY shell model and the black lines with no symbols
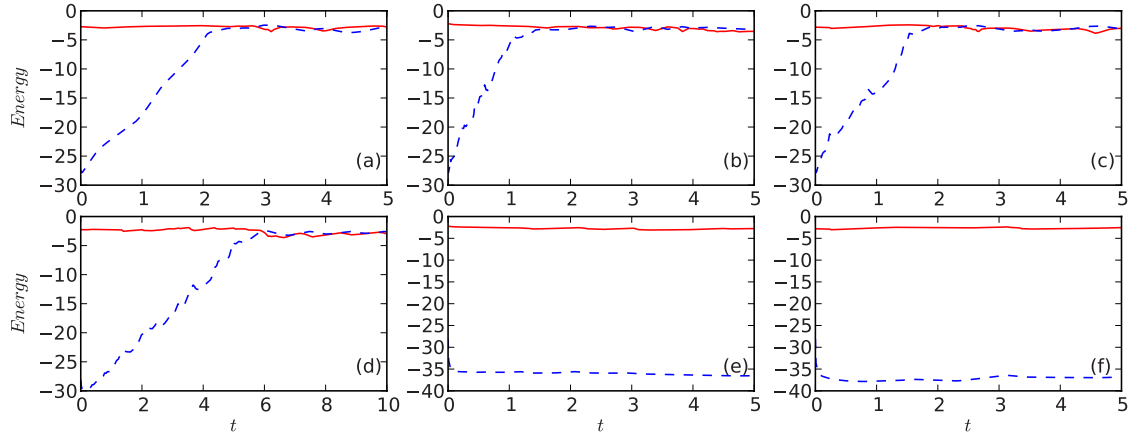
FIG. 2. (Color online) Semi-log (base 10) plots of the kinetic (red full curve) and magnetic (blue dashed curve) energies versus time for (a) $Pr_M = 10^2$ and $Re_M = 44\,870$; (b) $Pr_M = 1$ and $Re_M = 36\,361$; (c) $Pr_M = 10^{-1}$ and $Re_M = 52\,702$; (d) $Pr_M = 10^{-2}$ and $Re_M = 570$; (e) $Pr_M = 10^{-3}$ and $Re_M = 57$; and (f) $Pr_M = 10^{-4}$ and $Re_M = 63$. The values of ν are (a) 10^{-3}, (b) 10^{-5}, (c) 10^{-6}, (d) 10^{-5}, (e) 10^{-5}, and (f) 10^{-6}; and the magnetic-diffusion time $\tau_\eta = \ell_0^2 / \eta \simeq 2.52 \times 10^8$, 2.52×10^8, 2.52×10^8, 2.52×10^6, 2.52×10^5, and 2.52×10^5, respectively. Dynamo action occurs in (a)–(d) but not in (e) and (f).

show the K41 $k_n^{-5/3}$ spectrum for comparison. From this line we see that the NESS that is obtained, once dynamo action has occurred, is such that both velocity and magnetic-field

energy spectra display a substantial inertial range with K41 scaling; these inertial ranges are not large enough, at least near the dynamo boundary in our runs, for a reliable estima-
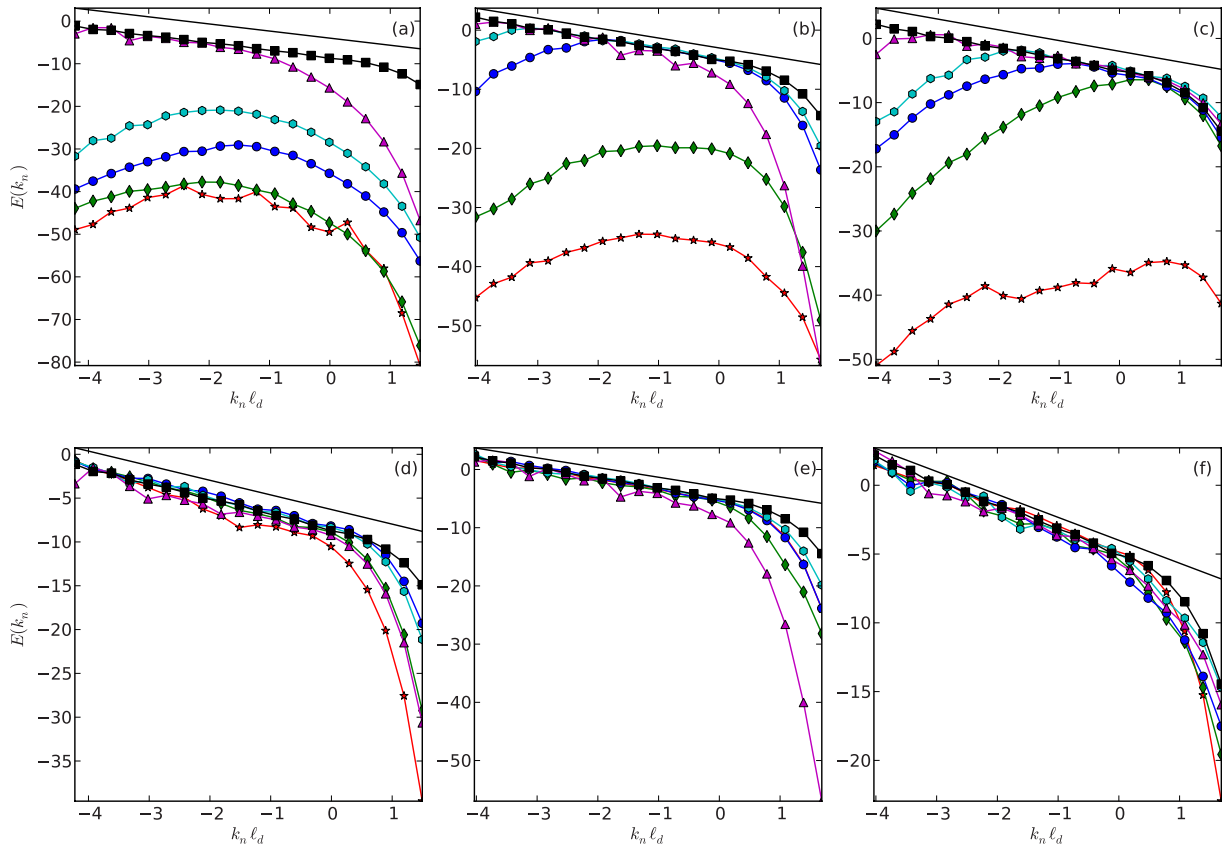

FIG. 3. (Color online) Log-log (base 10) plots showing the time evolution of the magnetic-energy spectrum $E_b(k_n)$ for representative parameter values at which dynamo action occurs: (a) $Pr_M = 10^{-2}$, $\nu = 10^{-7}$; (b) $Pr_M = 1$, $\nu = 10^{-5}$; (c) $Pr_M = 10^2$, $\nu = 10^{-5}$; analogous plots for kinetic-energy spectra are shown in (d), (e), and (f), respectively. The curves with red stars, green diamonds, blue hexagons, cyan circles, and magenta triangles are obtained, respectively, at $t = 1$, 5, 10, 15, and 100; the dissipation scale $\ell_d \simeq 7.422 \times 10^{-4}$ in (b), (c), (e), and (f); $\ell_d \simeq 4.779 \times 10^{-4}$ in (a) and (d). Curves with black squares indicate velocity spectra before the seed magnetic field is introduced; the full black line shows a $k^{-5/3}$ spectrum for comparison.
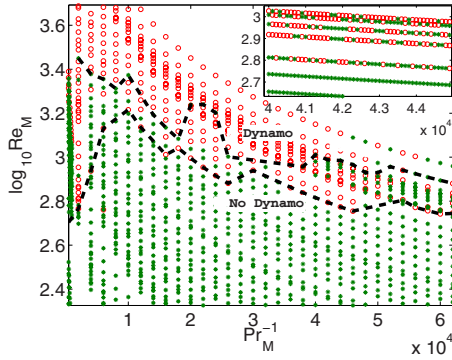
FIG. 4. (Color online) The dynamo stability diagram in the $(\mathrm{Pr}_M^{-1}, \mathrm{Re}_M)$ plane: red circles indicate dynamo action; green stars are used if no dynamo occurs. The boundary between the two regions shows an intricate, interleaved pattern of fine, dynamo, and no-dynamo regimes (see inset for a detailed view). We have drawn two black dashed lines; the region above the upper one of these lines is predominantly in the dynamo regime; the area below the lower one of these lines is principally in the no-dynamo regime.

tion of multiscaling corrections to the $-5/3$ exponent. If $\mathrm{Pr}_M \simeq 1$ then the scaling ranges in velocity and magnetic-field spectra are comparable; as Pr_M decreases (increases), the scaling range for the magnetic spectrum decreases (increases) relative to its counterpart in the velocity spectrum; these trends are clearly visible in the representative plots in Fig. 3.

We return now to the identification of the dynamo boundary. A close scrutiny of the plots in Fig. 2 shows that the initial growth of E_b is not monotonic. It is important, therefore, to set a threshold value of the magnetic energy E_b^c: for a given pair of values for Pr_M and Re_M, if $E_b(t) > E_b^c$ for $t > \tau_c$, where τ_c is the time at which the threshold value is crossed, we conclude that dynamo action occurs; if not, then there is no dynamo formation. By examining the growth of $E_b(t)$ we can, therefore, map out the dynamo boundary in the $(\mathrm{Pr}_M^{-1}, \mathrm{Re}_M)$ plane. The crossing time τ_c depends on Pr_M and Re_M.

Note that, if $\tau_c(\mathrm{Pr}_M, \mathrm{Re}_M) > t_{\max}$, the length of time for which we integrate Eqs. (3) and (4), we would conclude, *incorrectly*, that no dynamo action occurs for this of values of Pr_M and Re_M. In other words the dynamo boundary depends on $t_{\max}$; we have checked this explicitly in several cases.

An important questions arises now: is there a well-defined dynamo boundary in the $(\mathrm{Pr}_M^{-1}, \mathrm{Re}_M)$ plane as $t_{\max} \rightarrow \infty$? Earlier studies [7,16,20] have began to answer this question. They find that, if $t_{\max} \simeq \tau_\eta$, then a well-defined dynamo boundary is obtained. However, since they work with the MHD equations the error bars on this boundary are large and the range of values of Pr_M and Re_M rather limited.

The simplicity of our model allows us to carry out a systematic study of the dynamo boundary. We find that, at least in our shell model for MHD, we can obtain an asymptotic dynamo boundary (see Fig. 4) if we choose $E_b^c = 0.9 E_u$; i.e., we conclude that dynamo action has occurred if $E_b(t)$ exceeds $0.9 E_u$; furthermore, if $E_b(t)$ falls below 10^{-35} we say that dynamo action will never be achieved. We continue the

temporal evolution of Eqs. (3) and (4) until one of these criteria is satisfied. For all values of Pr_M and Re_M that we have used we find that this $t_{\max}$, the run time required to decide whether or not dynamo action occurs, is several orders of magnitude lower than τ_η. We have also checked for several representative pairs of values for Pr_M and Re_M that runs of length $t_{\max} \simeq \tau_\eta$ do not change our conclusions about such dynamo action.

The dynamo boundary that we obtain is shown in the stability diagram of Fig. 4. The red circles indicate parameter values at which we obtain dynamo action whereas green stars are used for values at which no dynamo occurs. The most important result that follows from this stability diagram is that the boundary between dynamo and no-dynamo regimes is very complicated. It seems to be of fractal-type, with an intricate pattern of fine dynamo regions interleaved with no-dynamo regimes. This is especially apparent in the inset of Fig. 4, which shows a detailed view of the stability diagram in the vicinity of the dynamo boundary. Earlier studies seem to have missed this fractal-type nature of the boundary because they have not been able to examine the transition in as much detail as we have for our shell model. However, fractal-type boundaries between different dynamical regimes have been suggested in other extended dynamical systems; recent examples include the transition to turbulence in pipe flow [35] and different forms of spiral-wave dynamics in mathematical models for cardiac tissue [36]. In dynamical systems a fractal basin boundary often separates the basin of attraction of a strange attractor from the basin of attraction of a fixed point or limit cycle; thus, a small change in the initial condition can lead either to chaos, associated with the strange attractor, or to the simple dynamical behaviors associated with fixed points or limit cycles. The shell-model equations we consider here are $4N$-dimensional dynamical systems, where N is the number of shells (the shell velocities and magnetic fields are complex); the complete basin boundaries for such a high-dimensional dynamical system (we use $N=30$ so $4N=120$) are not easy to determine; however, it is reasonable to assume that a complex, fractal-type boundary separates the basins of attraction of the dynamo and no-dynamo regimes, both of which display turbulence (and are, we presume, governed by strange attractors that lead to spatiotemporal chaos). In our study we do not change the initial condition; instead, we change the dynamical system by changing ν and η and hence Re_M and Pr_M^{-1}. This too affects the long-time evolution of the system as sensitively as does a change in the initial conditions because the fractal basin boundary itself changes with these parameters. Indeed, Ref. [35] has found this for the transition to turbulence and the edge of chaos in pipe flow; and Fig. 3 of Ref. [35] shows that the border in parameter space between the laminar and turbulent regions is very complicated in much the same way as the dynamo boundary is in our study. Furthermore, in Ref. [36], it has been shown that the dynamics of spiral waves of electrical activation depend sensitively on inhomogeneities in partial-differential-equation models for ventricular tissue; changes in the positions of these inhomogeneities in models for cardiac tissue correspond in our shell model to changes in parameters such as Pr_M and Re_M. In Fig. 4 we have drawn two black dashed lines; the region above the upper one of
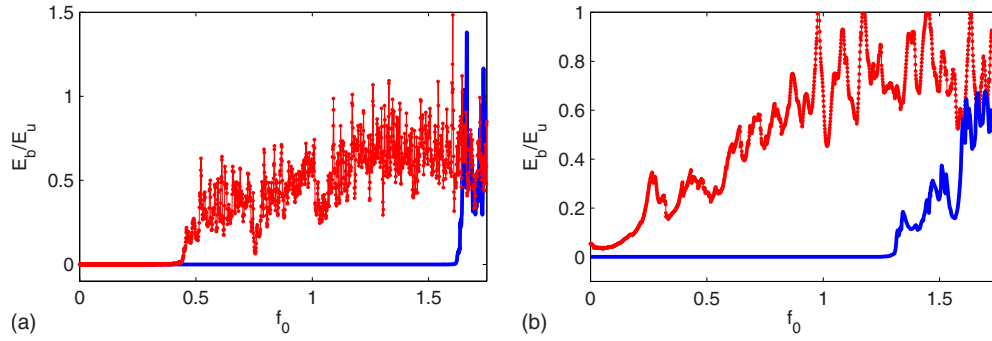
FIG. 5. (Color online) Plots of the dynamo order parameter E_b/E_u versus the forcing amplitude f_0 illustrating hysteretic behavior as f_0 is cycled across the dynamo boundary; here $\mathrm{Pr_M}=10^{-4}$ and $\nu=10^{-5}$. As f_0 increases, E_b/E_u follows the blue full line; if we now decrease f_0, then E_b/E_u follows the red dotted line and not the blue one; i.e., we have a hysteresis loop. We increase f_0 in steps of 1.0×10^{-3} from an initial value of 1.0×10^{-3}; we keep f_0 constant for a time duration 10 in (a) and 1 in (b); the red dotted-line segments of the hysteresis loops are obtained by decreasing f_0 at the same rates as for the blue full-line segments.

these lines is predominantly in the dynamo regime; the area below the lower one of these lines is predominantly in the no-dynamo regime. These two lines give an approximate indication of the error bars we might expect in the determination of the dynamo boundary in a study that cannot scan through points in the $(\mathrm{Pr_M^{-1}}, \mathrm{Re_M})$ plane as finely as we have.

From Fig. 1 we see that the order parameter E_b/E_u jumps from a very small value in the no-dynamo region to a value $\simeq 1$ in the dynamo state. It is natural, therefore, to think of the dynamo boundary as a nonequilibrium first-order boundary. In an equilibrium first-order transition the order parameter shows hysteretic behavior if we scan through a first-order boundary by, say, changing, at a finite rate, the field that is conjugate to the order parameter [30]. It is natural to ask if we see such hysteretic behavior at the dynamo boundary. Indeed, we do, as we show in Fig. 5 where we cross the dynamo boundary by changing the amplitude f_0 of the forcing term in Eq. (3). Figure 5 shows representative plots of the dynamo order parameter E_b/E_u versus f_0; these illustrate the hysteretic behavior that occurs when f_0 is cycled at a finite nonzero rate across the dynamo boundary; here $\mathrm{Pr_M} = 10^{-4}$ and $\nu = 10^{-5}$. As f_0 increases, E_b/E_u follows the blue full line: it increases and then saturates; fluctuations are superimposed on these mean trends. If we now decrease f_0, then E_b/E_u follows the red dotted line and not the blue one; i.e., we have a hysteresis loop. The faster the rate at which we change f_0 the wider is the hysteresis loop as is known from studies of hysteresis in spin systems [30]. Here we increase f_0 in steps of 1.0×10^{-3} from an initial value of 1.0×10^{-3}; we keep f_0 constant for a time period 10 in Fig. 5(a) and 1 in Fig. 5(b); the red dotted-line segments of the hysteresis loops are obtained by decreasing f_0 at the same rates as for the blue full-line segments; the loop in the former case is narrower than in the latter.

Given the analogy with first-order transitions that we have outlined above, it is natural to ask if nucleation-type phenomena [37] are also associated with dynamo formation. It would be interesting to check this in a DNS of the MHD equations. At the level of our shell model, the best we can do is to try to see if, for a given $\mathrm{Pr_M}$, when we obtain a dynamo, the time required for dynamo action τ_c diverges as we approach the dynamo boundary. Our data are consistent with an

increase in τ_c as we approach this boundary from the dynamo side as shown by the representative plots in Fig. 6. However, it is hard to fit a precise form to the behavior of τ_c near the dynamo boundary partly because of the complicated nature of this boundary which makes it difficult to estimate the position $\mathrm{Re_{Mb}}$ reliably (the plot in Fig. 6 is motivated by the form of Eq. (27) in Ref. [37]). The value of τ_c is not averaged in our simulations. It can depend on the specific realization, which follows from the initial condition, and on the threshold E_b^c. However, the main point we are making here is a qualitative one: as we approach the dynamo boundary from the dynamo side, the time τ_c required for dynamo action grows rapidly.

IV. CONCLUSIONS

We have presented a detailed study of dynamo action in a shell model of turbulence [23–25]. Our study has been designed to explore the nature of the boundary between dynamo and no-dynamo regimes in the $(\mathrm{Pr_M^{-1}}, \mathrm{Re_M})$ plane over a much wider range of $\mathrm{Pr_M}$ than has been attempted in earlier numerical studies. The dynamo boundary emerges as a first-order nonequilibrium phase boundary between one turbulent NESS and another [38]. This point of view is implicit in earlier work, e.g., in studies of the Kazantsev dynamo [39] or in studies that view dynamo generation as a subcritical bifur-
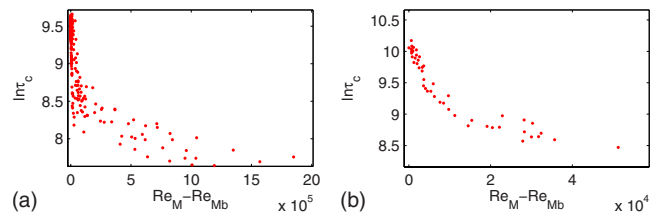

FIG. 6. (Color online) Representative plots of $\ln \tau_c$ versus $\mathrm{Re_M}-\mathrm{Re_{Mb}}$ for parameter values at which dynamo action occurs; here τ_c is in units of the time step δt and $\mathrm{Re_{Mb}}$ is the estimated position of the dynamo boundary: (a) $\mathrm{Pr_M}=1$ and (b) $\mathrm{Pr_M}=5\times10^{-4}$. Note that the time τ_c required for dynamo action increases rapidly as we approach the dynamo boundary (the plot here is motivated by Eq. (27) in Ref. [37]).

cation [31,40,41]. One of these studies [31] has remarked that when dynamo action "…is obtained in a fully turbulent system, where fluctuations are of the same order of magnitude as the mean flow…the traditional concept of amplitude equation may be ill-defined and one may have to generalize the notion of "subcritical transition" for turbulent flows…" We believe that the natural generalization is the nonequilibrium first-order transition we suggest above. We have explored the explicit consequences of such a view in far greater detail than has been attempted hitherto. In particular, the ratio E_b/E_u is a convenient order parameter for this nonequilibrium phase transition; it shows hysteresis across the dynamo boundary like order parameters at any first-order transition; and nucleation-type phenomena also seem to be associated with dynamo formation. Last, and perhaps most interesting, we find that the dynamo boundary seems to have a fractal character; this provides a natural explanation for the large error bars in earlier attempts to determine this boundary [7,16,27]. Furthermore, this fractal-type boundary might well be the root cause of magnetic-field reversals discussed, e.g., in Refs. [29,42].

It is important to check, of course, that our shell-model results carry over to the MHD equations. This requires large-scale DNS that might well be beyond present-day computing capabilities if we want to explore issues such as the possible fractal nature of the dynamo boundary. However, analogs of the hysteretic behavior we mention above have been obtained in DNS studies of the MHD equations [31,40,41]; hysteresis has also been seen in a numerical simulation that includes turbulent convection [43]. In some of these studies hysteretic behavior is obtained by changing the viscosity and thus the magnetic Prandtl number. We have obtained hysteresis by changing the forcing; this change in forcing might be easier to effect in experiments than a change in the viscosity or magnetic diffusivity.

To the best of our knowledge, earlier studies have not noted the increase in the dynamo-formation time τ_c as the dynamo boundary is approached from the dynamo side. We have suggested that this is akin to the increase in the time required to form a critical nucleus as we approach a first-order boundary [37]. It would be interesting to see if such an increase in τ_c can be obtained in DNS studies of dynamo formation with the MHD equations. It is worth noting here that some DNS studies [16] have suggested that simulation times comparable to the diffusion time scale τ_η are required to confirm dynamo formation; by contrast our shell-model study yields dynamo action on a much shorter time τ_c, which increases as we approach the dynamo boundary. Perhaps the large simulation times required for dynamo action in full MHD simulation might have arisen because these simulations have been carried out in the vicinity of the dynamo boundary.

To settle completely whether the dynamo boundary is of fractal type, very long simulations might be required to make sure that the apparent fractal nature is not an artifact of long-lived metastable states. To make sure that our calculations do not suffer from such an artifact, we have carried out very long runs for representative points in the region of the dynamo boundary in Fig. 4; we have found that these long runs do not change our results. Furthermore, it is useful to check whether, instead of one dynamo boundary, there is a sequence of transitions, with more and more complicated temporal behaviors for the order parameter, as has been seen in the turbulence-induced melting of a nonequilibrium vortex crystal [44]. We have not found any conclusive evidence for this but, in the vicinity of the dynamo boundary, the order parameter can oscillate for fairly long times (see, e.g., the green full curve in Fig. 1). To decide conclusively whether these oscillations characterize a new nonequilibrium oscillating state, different from the simple dynamo and no-dynamo NESSs we have mentioned, requires extensive numerical studies that lie beyond the scope of this paper.

In equilibrium statistical mechanics different ensembles are equivalent; in particular, we may determine a first-order phase boundary by using either the canonical or the grand-canonical ensemble. However, such an equivalence of ensembles does not apply to transitions between different NESSs; examples may be found in driven diffusive systems [45] or in the turbulence-induced melting of a nonequilibrium vortex crystal [44]. Given that the dynamo boundary separates two turbulent NESSs, we might expect that this boundary might depend on precisely how the system is forced. Evidence for this exists already: for example, the dynamo boundary depends on whether a stochastic external force is used [7] or whether a Taylor-Green force is used [16]; furthermore, this boundary is different if the flow is helical [21], as in most astrophysical dynamos. We hope our study of dynamo formation in a shell model for MHD will stimulate both DNS and experimental studies designed to explore the first-order nature of the dynamo transition.

[1] A. R. Choudhuri, *The Physics of Fluids and Plasmas: An Introduction for Astrophysicists* (Cambridge University Press, Cambridge, UK, 1998).

[2] G. Rüdiger and R. Hollerbach, *The Magnetic Universe: Geophysical and Astrophysical Dynamo Theory* (Wiley, Weinheim, 2004).

[3] H. Goedbloed and S. Poedts, *Principles of Magnetohydrodynamics with Applications to Laboratory and Astrophysical Plasmas* (Cambridge University Press, Cambridge, UK, 2004).

[4] D. Biskamp, *Magnetohydrodynamic Turbulence* (Cambridge University Press, Cambridge, UK, 2003).

[5] M. K. Verma, Phys. Rep. **401**, 229 (2004).

[6] S. Cowley, J.-F. Pinton, and A. Pouquet, New J. Phys. **9**, 244 (2007).

[7] A. A. Schekochihin *et al.*, New J. Phys. **4**, 84 (2002); A. A. Schekochihin, S. C. Cowley, J. L. Maron, and J. C. McWilliams, Phys. Rev. Lett. **92**, 054502 (2004); New J. Phys. **9**, 300 (2007); A. A. Schekochihin, S. C. Cowley, and S. F. Taylor, Astrophys. J. **612**, 276 (2004).

[8] P. H. Roberts and G. A. Glatzmaier, Rev. Mod. Phys. **72**, 1081 (2000).

[9] F. Pétrélis and S. Fauve, Europhys. Lett. **22**, 273 (2001); **76**, 602 (2006); S. Fauve and F. Pétrélis, in *Peyresq Lectures on Nonlinear Phenomena*, edited by J.-A. Sepulchre (World Scientific, Singapore, 2003), Vol. 2, p. 164; S. Fauve and F. Pétrélis, C. R. Phys. **8**, 87 (2007).

[10] A. Gailitis *et al.*, Phys. Rev. Lett. **84**, 4365 (2000); A. Gailitis, O. Lielausis, E. Platacis, S. Dementev, A. Cifersons, G. Gerbeth, T. Gundrum, F. Stefani, M. Christen, and G. Will, *ibid.* **86**, 3024 (2001); Rev. Mod. Phys. **74**, 973 (2002); Surv. Geophys. **24**, 247 (2003); Phys. Plasmas **11**, 2838 (2004).

[11] R. Stieglitz and U. Müller, Phys. Fluids **13**, 561 (2001); U. Müller, R. Stieglitz, and S. Horanyi, J. Fluid Mech. **498**, 31 (2004); U. Müller and R. Stieglitz, Nonlinear Processes Geophys. **9**, 165 (2002).

[12] N. L. Peffley, A. B. Cawthorne, and D. P. Lathrop, Phys. Rev. E **61**, 5287 (2000); W. L. Shew and D. P. Lathrop, Phys. Earth Planet. Inter. **153**, 136 (2005).

[13] M. Bourgoin *et al.*, Phys. Fluids **14**, 3046 (2002); **16**, 2529 (2004); L. Marié *et al.*, Magnetohydrodynamics **38**, 163 (2002); R. Monchaux *et al.*, Phys. Rev. Lett. **98**, 044502 (2007).

[14] A. Kolmogorov, Dokl. Akad. Nauk SSSR **31**, 538 (1941); Proc. R. Soc. London, Ser. A **434**, 15 (1991).

[15] S. Boldyrev and F. Cattaneo, Phys. Rev. Lett. **92**, 144501 (2004).

[16] Y. Ponty, H. Politano, and J.-F. Pinton, Phys. Rev. Lett. **92**, 144503 (2004); Y. Ponty, P. D. Mininni, D. C. Montgomery, J. F. Pinton, H. Politano, and A. Pouquet, *ibid.* **94**, 164502 (2005); New J. Phys. **9**, 296 (2007).

[17] S. Kenjereš and K. Hanjalić, Phys. Rev. Lett. **98**, 104501 (2007); New J. Phys. **9**, 306 (2007).

[18] M. Meneguzzi, U. Frisch, and A. Pouquet, Phys. Rev. Lett. **47**, 1060 (1981); J. Léorat, A. Pouquet, and U. Frisch, J. Fluid Mech. **104**, 419 (1981).

[19] H. Chou, Astrophys. J. **556**, 1038 (2001).

[20] P. D. Mininni, D. C. Montgomery, and A. Pouquet, Phys. Fluids **17**, 035112 (2005); P. D. Mininni *et al.*, Astrophys. J. **626**, 853 (2005); P. Mininni, A. Alexakis, and A. Pouquet, Phys. Rev. E **72**, 046302 (2005); P. D. Mininni and A. Pouquet, Phys. Rev. Lett. **99**, 254502 (2007).

[21] A. Brandenburg, Astrophys. J. **697**, 1206 (2009).

[22] A. B. Iskakov, A. A. Schekochihin, S. C. Cowley, J. C. McWilliams, and M. R. E. Proctor, Phys. Rev. Lett. **98**, 208501 (2007).

[23] A. Basu, A. Sain, S. K. Dhar, and R. Pandit, Phys. Rev. Lett. **81**, 2687 (1998); C. Kalelkar and R. Pandit, Phys. Rev. E **69**, 046304 (2004).

[24] P. Frick and D. Sokoloff, Phys. Rev. E **57**, 4155 (1998); S. A. Lozhkin, D. D. Sokolov, and P. G. Frick, Astron. Rep. **43**, 753 (1999).

[25] A. Brandenburg, K. Enqvist, and P. Olesen, Phys. Rev. D **54**, 1291 (1996).

[26] P. Giuliani and V. Carbone, Europhys. Lett. **43**, 527 (1998).

[27] J. Leorat, P. Lallemand, J. L. Guermond, and F. Plunian, in *Dynamo and Dynamics: A Mathematical Challenge*, edited by P. Chossat *et al.* (Kluwer Academic, Dordrecht, 2001), pp. 25–33; R. Stepanov and F. Plunian, J. Turbul. **7**, 39 (2006).

[28] M. K. Verma, T. Lessinnes, D. Carati, I. Sarris, K. Kumar, and M. Singh, Phys. Rev. E **78**, 036409 (2008).

[29] R. Benzi and J. Pinton, e-print arXiv:0906.0427.

[30] M. Rao, H. R. Krishnamurthy, and R. Pandit, J. Phys.: Condens. Matter **1**, 9061 (1989); Phys. Rev. B **42**, 856 (1990).

[31] Y. Ponty, J. P. Laval, B. Dubrulle, F. Daviaud, and J. F. Pinton, Phys. Rev. Lett. **99**, 224501 (2007).

[32] T. Bohr, M. H. Jensen, G. Paladin, and A. Vulpiani, *Dynamical Systems Approach to Turbulence* (Cambridge University, Cambridge, UK, 1998).

[33] E. Gledzer, Sov. Phys. Dokl. **18**, 216 (1973); K. Ohkitani and M. Yamada, Prog. Theor. Phys. **81**, 329 (1989).

[34] P. Perlekar and R. Pandit, New J. Phys. **11**, 073003 (2009).

[35] T. M. Schneider, B. Eckhardt, and J. A. Yorke, Phys. Rev. Lett. **99**, 034502 (2007).

[36] T. K. Shajahan, S. Sinha, and R. Pandit, Phys. Rev. E **75**, 011929 (2007); T. K. Shajahan, A. R. Nayak, and R. Pandit, PLoS ONE **4**, e4738 (2009).

[37] D. W. Oxtoby, J. Phys.: Condens. Matter **4**, 7627 (1992).

[38] We use the expression first-order transition as in equilibrium statistical mechanics since the order parameter (the first derivative of a free energy) jumps at the transition. Since there is no free energy for the NESSs we consider, one can, just as well, refer to this as a discontinuous transition.

[39] For example, see the following: A. P. Kazantsev, Sov. Phys. JETP **26**, 1031 (1968); D. Vincenzi, J. Stat. Phys. **106**, 1073 (2002); A. A. Schekochihin, S. C. Cowley, S. F. Taylor, G. W. Hammett, J. L. Maron, and J. C. McWilliams, Phys. Rev. Lett. **92**, 084504 (2004).

[40] F. J. Busse, J. Geophys. **43**, 441 (1977).

[41] W. Kuang, W. Jiang, and T. Wang, Geophys. Res. Lett. **35**, L14204 (2008).

[42] M. Bourgoin, R. Volk, N. Plihon, P. Augier, and J.-F. Pinton, New J. Phys. **8**, 329 (2006).

[43] R. D. Simitev and F. H. Busse, Europhys. Lett. **85**, 19001 (2009).

[44] P. Perlekar and R. Pandit, New J. Phys. **12**, 023033 (2010).

[45] M. Acharyya, A. Basu, R. Pandit, and S. Ramaswamy, Phys. Rev. E **61**, 1139 (2000).